Engineering and Technology Journal
Journal homepage: https://etj.uotechnology.edu.iq

Investigating The Effect of Various Parameters on The Yield of Graphene Obtained Through Graphite Exfoliation Using CO_2 Supercritical Fluid

Shahab A. Saeedi, Javad Sargolzaei*

Department of Chemical Engineering, Faculty of Engineering, Ferdowsi University of Mashhad, Mashhad, Iran
*Corresponding author Email: Sargolzaei@um.ac.ir

HIGHLIGHTS

- Conventional methods of graphene production are time-consuming and expensive.
- The parameters affecting the extraction of graphene from graphite were investigated using Supercritical CO_2.
- Additives used in the synthesis process have the role of deactivating the surface.
- The test design was done with "Design Expert" software and then tested in the laboratory.
- The software results were in high agreement with the laboratory results, and mono/bilayer graphene was obtained.

ARTICLE INFO

Handling editor: Qusay F. Alsalhy

Keywords:
Graphite; $scCO_2$; Exfoliation; Characterization; Design Expert.

ABSTRACT

Due to its high penetration force and low viscosity, the Supercritical carbon dioxide ($scCO_2$) can spread between the graphite layers, overcome van der Waals forces, and transform graphite into multilayer graphene. The results of the test plan with the Design Expert software and also the use of these results in the laboratory showed that the parameters of temperature, pressure, initial amount of graphite, addition of surfactant and solvent auxiliary, the duration of sample placement in the device, the duration of carbon dioxide gas release from the device, and the time and power of ultrasonic and centrifuge operations can accelerate the exfoliation process. The resulting graphene was characterized by TEM, RAMAN, XRD, and AFM techniques. Based on the obtained results, it was found that mono/bilayer graphene was obtained by applying optimum conditions. The results confirmed the formation of mono/bilayer graphene based on the G-Band of 1583 cm^{-1} in the Raman test, a wavelength of 26.44° in the XRD test, and a thickness of 1.5 nm in the AFM test. With a simple, low-cost approach, this method, without using toxic and expensive chemicals with high profitability, can replace other complex graphene production methods, such as chemical vapor leakage and plasma etching, and be chemically reduced.

.

1. Introduction

Since the discovery of graphene in 2004, graphene has attracted attention due to its attractive electronic, thermal, optical, and mechanical properties in various applications such as electronics, food industry, energy, etc. [1-4]. Currently, various methods for preparing graphene have been reported, all with the general goal of exploring the unique properties of graphene to increase potential practical applications. But, each of these methods has its disadvantages [5]. For example, high-quality graphene can be obtained through micromechanical cleavage, but this method is very expensive and time-consuming for mass production [6]. Also, graphene can be prepared by co-growth on a SiC substrate and by chemical vapor deposition (CVD) on metal substrates. Still, these methods lead to non-uniform products, make transfer difficult, and are expensive [7]. Another method of producing graphene is called chemical reduction of graphene oxide (RGO), but this method also has disadvantages. In fact, the aggressive oxidation process of graphite introduces oxygen-containing groups and hydroxyl (-OH), carbonyl (-COOH), and epoxide groups into the graphene base plate and further causes structural defects in the SP^2 bond network and damages the electronic performance of graphene [8]. Recently, extraction with supercritical fluid due to its low viscosity [9], high permeability, short extraction time [10], a method with very low toxicity and non-flammability [11], no contamination of the product with solvent [12], environment friendly, performing extraction operations at low temperatures (to preserve the properties temperature-sensitive materials) [13] and the easy recovery of the final product have received much attention, which results in

http://doi.org/10.30684/etj.2023.143211.1569
Received 08 September 2023; Received in revised form 08 October 2023; Accepted 13 October 2023; Available online 31 December 2023
2412-0758/University of Technology-Iraq, Baghdad, Iraq

high efficiency and profitability. Ahangari et al. [14], reported for the first time that graphite can be layered and separated in graphene sheets in the $scCO_2$. Still, considering that only surfactant was added during the experiment and without any help, no solvent was used, and at the end of the experiment, ultrasonic and centrifuge operations were not used, the added surfactant was hardly removed from the final product. Also, the obtained graphene had 10 layers, and the production efficiency was about 2% [15].

Gao et al. and Sun et al. [16,17] reviewed the various SCFs method (such as ethanol and NMP) have been explored to exfoliate graphite, but their applications were limited due to harsh conditions. As an excellent green substitute for conventional organic solvents, $scCO_2$ has a wide range of applications due to its lower critical point, making reaching the supercritical state easier [18,19]. Compared with general solvents, CO_2 is inexpensive, non-toxic, recyclable, and reusable, and has a wide range of uses in food, medical, and chemical industries [20]. Yu et al. [21], produced defect-free graphene using different agitators (type, diameter) in NMP with the help of $scCO_2$ intercalation. When a straight impeller combined with a nonperforated draft tube was used, the proportion of 1-3 layers was about 56.4% [22].

Previous research has not discussed the simultaneous use of the Design Expert software and the use of the results of this software in the laboratory by the $scCO_2$. Also, the effective and optimal parameters for the preparation of few-layer graphene are investigated, such as temperature parameters, pressure, an initial amount of graphite, the addition of co-solvents DMF, NMP, and Isopropanol, the addition of surfactants sodium hexametaphosphate and sodium lignosulfonate, Exfoliation duration in the cell, Carbon dioxide discharge rate, and performance of ultrasonic and centrifugation processes and comparison the soft results were not performed in a laboratory. This article discusses the above parameters and characterization of graphene prepared from graphite.

2. Materials and Methods

2.1 Materials and Equipment

Devices applied in the experiments include a supercritical fluid device (made in the Food Industry Research Laboratory, Department of Chemical Engineering, Ferdowsi University of Mashhad, Iran), Carbon dioxide (Purity >99.5%, Shanghai high-tech Co, China), Electronic balance (ALE-223, M.T. Electronic, Germany), Oven (ATP-G23, Shimaz Co, Iran), Ultrasonic device (DSA-150-SK, Camel, Germany), Centrifuge device (GUR-3200, Camel, Germany).

Materials applied in the experiments include Graphite (99.99%, Merck, Germany), Sodium hexametaphosphate (99%, Riedel, Germany), Sodium lignosulfonate (99%, Riedel, Germany), *N*-Methyl pyrrolidone (NMP) (1.25 M, Mojalali Co, Iran), Dimethylformamide (DMF) (1.26 M, Mojalali Co, Iran), Isopropanol (1.25 M, Mojalali Co, Iran), Filter paper (Whatman, Germany).

2.2 Design Expert

The response surface method designs the test matrix based on the number of variables and each variable's maximum and minimum limits. In this way, the variable levels in each test and their number are determined. The arrangement in the design of experiments is such that reliable statistical results can be obtained even if the test is not repeated. Thus, this method facilitates the research approach and reduces the time and other side costs. On the other hand, it can evaluate the interaction of parameters [23]. Process variables were selected based on preliminary testing. The statistical table of variables analysis was determined for the experimental data using Design Expert 7.0 software. The response surface method is cost-effective and reliable for optimizing certain processes. This method decreases the number of required tests [24]. The Box Behnken test assessed the parameters affecting the response rate. To get a mathematical model, the Box Behnken design with seven variables and three repetitions in the central point of the design was utilized in this research to determine the effect of temperature, pressure, initial amount of graphite, the addition of co-solvents (DMF) and surfactants (Sodium hexametaphosphate), exfoliation duration in the cell, and carbon dioxide discharge time as shown in Table 1.

Very little research has been done on experiment design using Design Expert software to investigate effective parameters in graphene synthesis using $scCO_2$ fluid and the effect of these parameters on increasing graphene efficiency. In the above articles, the tests were limited due to the long analysis time, large number of test steps, and high cost, and only 2 to 4 effective factors were studied. Still, in this article, all effective parameters in the synthesis of graphene are discussed and studied without limitations [23,24].

Table 1: Levels and the experimental condition for Box Behnken design

Factor	Units	Type	Changes	Std. Dev.	Low level (-)	High level (+)
Temperature	℃	Factor	Easy	0	30	60
Pressure	Bar	Factor	Easy	0	10	300
Exfoliation duration in the cell: T (1)	hr	Factor	Easy	0	1	2
Carbon dioxide discharge time: T (2)	Sec	Factor	Easy	0	5	30
Amount of Di Methyl Formamide (DMF)	g	Factor	Easy	0	0.02	0.2
Amount of Sodium hexametaphosphate	g	Factor	Easy	0	0.02	0.2
Initial amount of Graphite	g	Factor	Easy	0	1	5
R_1		Response		21.8942	0.8	126

2.2.1 Box-Behnken test design table in design expert software

Table 2 shows the experiment design designed by the Box-Behnken method for seven factors, which runs 46 experiments.

Table 2: Experimental runs for Box-Behnken design

Run	Factor A Temperature (℃)	Factor B Pressure (Bar)	Factor C Exfoliation duration in the cell (hr)	Factor D Carbon dioxide discharge time (Sec)	Factor E Amount of DMF (g)	Factor F Amount of Sodium hexameta phosphate (g)	Factor G Initial amount of Graphite (g)	Factor H Response
1	60	300	1.28	5	0.02	0.173	4.2	117
2	60	10	2	5	0.2	0.0551	1	1.04
3	55.5	79.6	1.935	30	0.2	0.1415	5	30
4	55.05	227.5	1	21.125	0.1235	0.092	5	47
5	30	95.55	1.57	5	0.1352	0.0965	2.8	22
6	30	10	1.35	18.75	0.02	0.02	1	119
7	36.3	10	1.01	30	0.145281	0.2	4.92	1.01
8	30	256.5	1.65	16.25	0.0407	0.056	5	120
9	48.15	108.6	1	12.75	0.2	0.02	1.4	1
10	30	292.75	2	5	0.2	0.2	5	26
11	60	10	1.055	30	0.02	0.2	5	31
12	45	10	1	5	0.02	0.0353	5	59
13	30	147.75	1	13	0.0209	0.2	3.84784	0.8
14	60	141.95	1.6	5	0.2	0.02	5	24
15	30	10	1.77	22.75	0.2	0.2	1.38	22
16	43.8	10	1	30	0.1037	0.1397	1.26	0.9
17	30	39	2	30	0.02	0.1208	3.6	38
18	30	300	2	5	0.02	0.2	1	1.2
19	60	10	1	5	0.02	0.191	1	35
20	60	300	1.48	5	0.0983	0.02	1	35
21	47.4	130.35	2	6.625	0.02	0.02	2.91073	60
22	60	300	2	30	0.02	0.02	5	27
23	45	198.5	1.42	5	0.1676	0.2	1	56
24	46.5	300	1.72	17.875	0.2	0.083	2.98	126
25	33.3	220.25	2	30	0.1631	0.02	1	123
26	60	300	1.75	30	0.1271	0.02	1	44
27	42	300	1	30	0.02	0.02	2.66	61
28	39.45	300	1.525	30	0.101	0.2	4.12	53
29	60	181.209	2	16.25	0.11	0.2	2.62	32
30	46.5	300	1.72	17.875	0.2	0.083	2.98	117
31	43.5	10	1.83	5	0.029	0.2	5	1.04
32	38.55	256.5	1	5	0.02	0.0983503	1.02	30
33	51.9	10	1	9.125	0.2	0.1865	4.4	47
34	30	82.5	1.05	30	0.2	0.0326	5	22
35	37.5	10	2	15.375	0.1604	0.02	5	119
36	30	95.55	1.57	5	0.1352	0.0965	2.8	1.01
37	30.6	300	1	5	0.2	0.02	5	120
38	60	300	1	30	0.2	0.2	1	1
39	30	300	1.97	27.4012	0.0209	0.117015	1.71885	26
40	54.45	172.4	1.605	23.875	0.02	0.1199	1	31
41	30	300	1	20.625	0.1649	0.1289	1	59
42	60	10	1.475	27.125	0.1037	0.02	2.94	0.8
43	54.45	172.4	1.605	23.875	0.02	0.1199	1	24
44	33.75	10	1	29.375	0.02	0.0587	4.8	22
45	55.05	227.5	1	21.125	0.1235	0.092	5	0.9
46	60	181.209	2	16.25	0.11	0.2	2.62	38

2.2.2 Optimization employing Box behnken design

Forty-six experiments were designed by the software. The list of designed experiments and the points determined in each experiment are presented in Table 3.

According to the prediction of Design Expert software, Quadratic was selected as a polynomial model. The obtained ANOVA Table (Table 3) was analyzed based on p (probability) values where *p*-values smaller than 0.05 imply the influence of the relevant factor. The term with a higher *F*-value and lower *p*-value is more significant.

Based on Table 3, the *p*-value < 0.05 indicates the acceptable model conditions, while values greater than 0.05 suggest that the model conditions are insignificant. To predict the adequacy of the designed model, *p*-values and Lack of Fit were considered

in which the *p*-value should be less than 0.05 (Significant) and the Lack of Fit should be greater than 0.05 (Not significant). This holds for the response, suggesting that the designed model is suitable.

Table 3: Statistical analysis result of entrapment efficiency

Source	Sum of Squares	df	Mean Square	*F*-value	*p*-value	
Model	67958.18	35	1941.66	4.05	0.0115	Significant
Factor A: Temperature (°C)	2497.05	1	2497.05	5.21	0.0456	
Factor B: Pressure (Bar)	9557.73	1	9557.73	19.94	0.0012	
Factor C: Exfoliation duration in the cell (hr)	3865.19	1	3865.19	8.06	0.0176	
Factor D: Carbon dioxide discharge time (Sec)	854.27	1	854.27	1.78	0.2115	
Factor E: Amount of DMF (g)	90.64	1	90.64	0.1891	0.6729	
Factor F: Amount of sodium hexameta phosphate (g)	4871.05	1	4871.05	10.16	0.2097	
Factor G: Initial amount of Graphite (g)	1080.39	1	1080.39	2.25	0.0164	
AB	65.64	1	65.64	0.1369	0.7191	
AC	62.99	1	62.99	0.1314	0.7245	
AD	1253.91	1	1253.91	2.62	0.1369	
AE	14.07	1	14.07	0.0293	0.8674	
AF	15897.49	1	15897.49	33.16	0.3002	
AG	433.53	1	433.53	0.9044	0.0364	
BC	367.18	1	367.18	0.7660	0.4020	
BD	2418.61	1	2418.61	5.05	0.0485	
BE	534.83	1	534.83	1.12	0.3157	
BF	1.23	1	1.23	0.0026	0.9606	
BG	355.08	1	355.08	0.7408	0.4096	
CD	2334.47	1	2334.47	4.87	0.0518	
CE	1286.79	1	1286.79	2.68	0.1324	
CF	5021.97	1	5021.97	10.48	0.1189	
CG	794.58	1	794.58	1.66	0.0126	
DE	27.78	1	27.78	0.0579	0.8146	
DF	290.28	1	290.28	0.6056	0.4545	
DG	274.68	1	274.68	0.5730	0.4665	
EF	185.49	1	185.49	0.3870	0.5478	
EG	6.28	1	6.28	0.0131	0.9111	
FG	20.78	1	20.78	0.0433	0.8393	
A^2	3677.71	1	3677.71	7.67	0.0198	
B^2	4815.80	1	4815.80	10.05	0.0100	
C^2	2552.15	1	2552.15	5.32	0.0437	
D^2	3809.49	1	3809.49	7.95	0.0182	
E^2	22.00	1	22.00	0.0459	0.8347	
F^2	1625.53	1	1625.53	3.39	0.0954	
G^2	38.05	1	38.05	0.0794	0.7839	
Residual	4793.55	10	479.36			
Lack of Fit	3427.66	5	685.53	2.51	0.1677	Not significant
Pure Error	1365.90	5	273.18			
Cor Total	72751.73	45				

The nonlinear quadratic model Equation 1 shown below can be used to calculate the expected Y response:

$$Y = \alpha 0 + \alpha 1A + \alpha 2B + \alpha 3C + \alpha 1\alpha 1A2 + \alpha 2\alpha 2B2 + \alpha 3\,\alpha 3C2 + \alpha 1\alpha 2AB + \alpha 1\alpha 3AC + \alpha 2\alpha 3BC \quad (1)$$

The model expressions A, B, C, D, G, A^2, B^2, C^2, D^2, AG, BD, and CG are important, as shown in Table 3. The final Equation 2 in terms of real factors is as follows:

$$Y = -276.869 + 6.705A - 0.111B + 277.872C + 5.973D - 1059.111G + 24.811AG - 0.007BD - 409.296CG - 0.110A2 + 0.001B2 - 80.886C2 - 0.154D2 \quad (2)$$

The influence of the independent variables and their joint effects are presented in Pareto charts, shown in Figure 1. In these graphs, the influence of the variables is denoted by the bar length. The time when pressure has the greatest effect on the exfoliation process (24.46), then the carbon dioxide gas discharge time (17.42), and similarly the exfoliation time in the supercritical fluid device tube (17.42), the initial amount of graphite (15.49). Also, the Pareto diagram shows that the carbon

dioxide discharge time and temperature parameters had no effect. When the effect of temperature parameters and the amount of initial graphite is used as a component, it does not have an effective effect. Still, when the pressure and time of carbon dioxide gas discharge are used together, it acts as an effective parameter in exfoliation (9.51). Also, the square effect of B and D parameters did not have a good effect on peeling (-3.18 and -2.74), but the square effect of A and C parameters (5.93 and 1.24) had a significant effect [25,26].

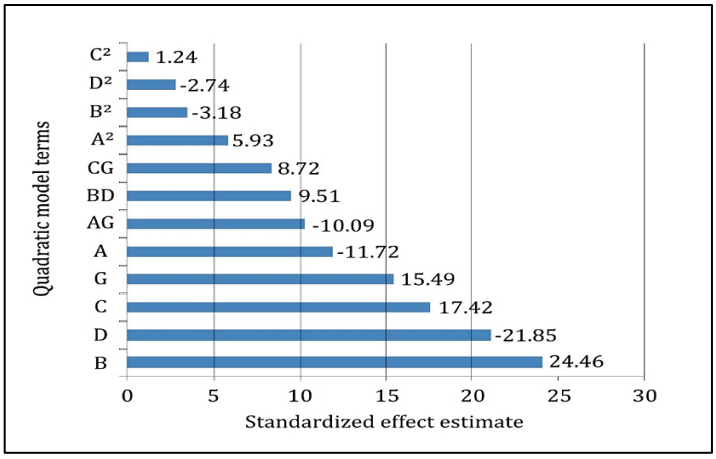

Figure 1: Pareto chart for parameters of exfoliation

Table 4 shows that R^2 and Adjusted R^2 values are also important. The closer they are to 1, the more adequate the model is. The software-proposed model is Quadratic, and the results of Fit Statistics are listed in Table 4.

Table 4: Results of Fit Statistics

Std. Dev.	Mean	C.V.%	R^2	Adjusted R^2	Predicted R^2	Adeq Precision
21.89	42.88	51.05	0.9916	0.9901	-4.5761	7.3290

According to the Design Expert results, the optimal conditions to achieve the highest yield of graphene include:

A temperature of 45˚C, a pressure of 155 bar, an initial graphite amount of 3 g, the addition of 0.1 g sodium hexametaphosphate as a surfactant, and 0.1 g DMF as a co-solvent, 1.5 hr of placing the sample inside the device for exfoliation and discharge of carbon dioxide from the device in 17.5 sec.

2.3 Sample Preparation and Experimentation

In the first step, Graphite (1, 2,3, and 5 g) was weighed on a filter paper, which was placed onto a Petri dish, and different co-solvents (NMP, DMF, and Isopropanol), and then distilled water was added. Next, different surfactants (in the first case, 0.1 g sodium hexametaphosphate, and in the second case, 0.1 g sodium lignosulfonate) were mixed with the mixture. The mixture was wrapped in filter paper and placed in the cell of the supercritical fluid device. The exfoliation process was carried out under high pressure inside the stainless steel cell. To begin the process, the device was set at different temperatures (35, 45, 50, and 60 ˚C) and pressures (10, 50, 155, 250, and 300 bar), and $scCO_2$ was released. Once the device provided the required pressure, it was turned off, and exfoliation was conducted for two different durations (1, 1.5, and 2 hr). Then, the carbon dioxide gas in the device was discharged using the discharge valve. To investigate the effect of discharge rate on graphene quality and yield, the gas was discharged in 5, 17.5, and 30 sec. After the sample was taken out of the cell, it was placed in the ultrasonic device and then the centrifuge for different durations (0-240 min ultrasonication and 0-120 min centrifugation) at different powers (0-300 W) and different speeds (0-2000 rpm). Finally, the obtained samples were characterized. Figure 2 shows a schematic of the supercritical fluid device in which $scCO_2$ fluid was utilized to produce graphene out of graphite [12].

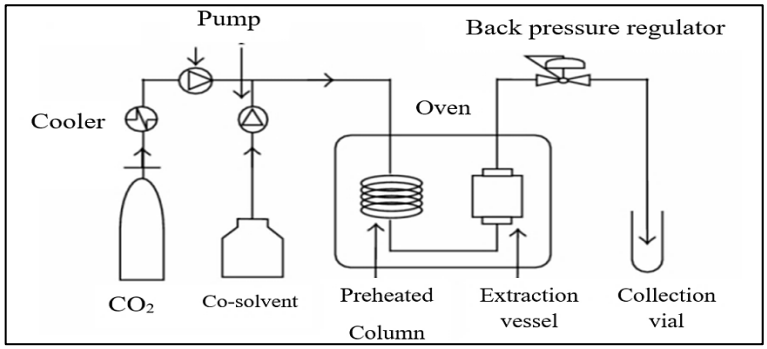

Figure 2: Schematic of the carbon dioxide supercritical fluid device [12]

3. Results and Discussion

3.1 Effect of Different Operational Parameters on The Quality and Yield of Graphene

3.1.1 Temperature and pressure

Experiments were carried out at temperatures 35, 45, 50, and 60°C and 10, 50, 155, 250, and 300 bar pressures. During the exfoliation process of graphite, when the temperature increases, the energy of the CO_2 molecules is increased, so it can overcome the van der Waals forces between the graphite layers and increase the graphene yield [27].

As pressure is a crucial parameter for the exfoliation of graphite into graphene, its influence on graphene yield was investigated. This increase in yield results from, as the pressure is increased, more CO_2 molecules intercalated and accumulating in the interlayer of graphite due to a good compressibility of $scCO_2$, which then generates a stronger repulsive free energy barrier that expands the space between the interlayers and, thus, results in an easier formation of graphene sheets. The space of the interlayer of graphite (0.335 nm) is large enough for the CO_2 molecule (0.233 nm) to enter. The size of the gap is around 0.102 nm. Thus, the CO_2 molecule can diffuse into the interlayers of graphite. Moreover, this increase in pressure and the resulting higher free energy barrier and reduced attraction can also enhance the dispersion stability of graphene sheets. As a result, the yield is enhanced with increasing pressure. Still, it is noticed that the yield decreases to 49% when the pressure increases from 250 to 300 bar, which might be attributed to the counteraction between the higher pressure and the cavitation effect of ultrasonication. In other words, higher acoustic pressure and increasing power are needed to produce the desired cavitation. The ultrasound role is suppressed at the higher pressure, so the yield decreases [28].

This research obtained the optimum temperature and pressure at 50°C and 250 bar, respectively. According to Figure 3, with the increase of temperature from 35°C to 50°C, the efficiency of graphene increased from 23% to 52%. Still, with the increase of temperature from 50°C to 60°C, the efficiency of graphene decreased significantly. The reason is that the carbon starts to burn at temperatures above 50°C, resulting in reduced efficiency. Also, according to Figure 4, by increasing the pressure from 10 bar to 250 bar, the efficiency of graphene increased from 17% to 55%, but with the increase of pressure from 250 bar to 300 bar, the efficiency of graphene decreased from 55% to 49%. The reason is that at pressures higher than 250 bar, the density of the solvent is reduced, it becomes more difficult to penetrate between the layers, and the separated layers accumulate again and form graphite, which decreases graphene efficiency.

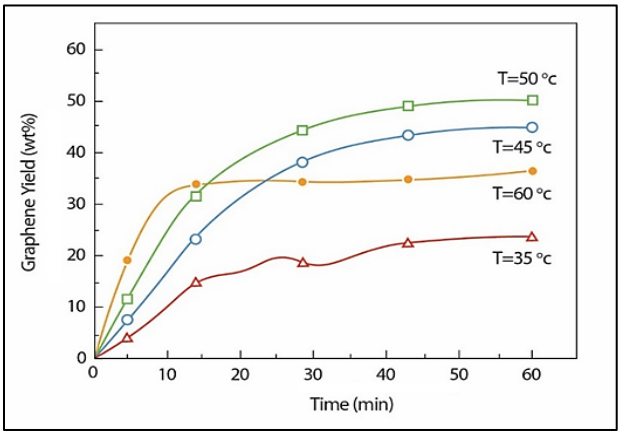

Figure 3: Effect of temperature on the yield of graphene

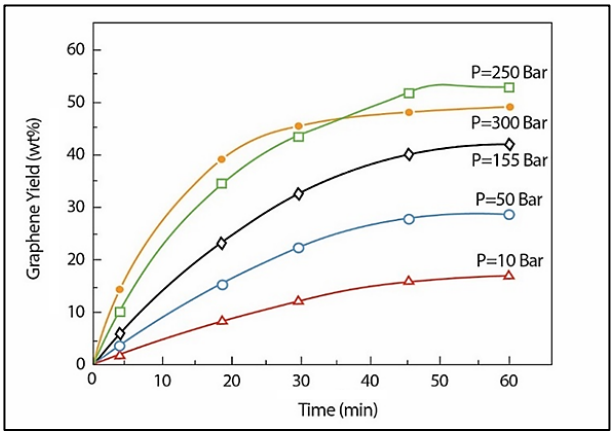

Figure 4: Effect of pressure on the yield of graphene

3.1.2 Initial amount of graphite

Experiments were conducted using 1, 2, 3, and 5 g raw graphite. As shown in Figure 5, the yield reduces from 36% to 20% as the initial amount increases from 2 to 3 g. This could be because the amount of CO_2 interacting between the interlayers of graphite was not enough to either expand the interlayer spacing or provide a higher free energy barrier that would have stabilized the graphene sheets. This suggests that the ratio between the CO_2 amount and the initial graphite amount is also an important factor affecting graphene yield from graphite's exfoliation [29].

Figure 5 shows the effect of the initial amount of graphite on the yield of graphene. It can be seen that there is an optimum amount for the graphite used in the experiments. So, graphite should be low enough to ensure better exfoliation and graphene extraction. However, the amount of graphite should be high enough to ensure that the effects of different additives and the $scCO_2$ can be observed. It should be noted that a large amount of graphite causes processing problems in the device and increases the need for extraction fluid and side costs [30]. In this article, the optimum amount of raw graphite was 2 g, resulting in the highest yield of graphene.

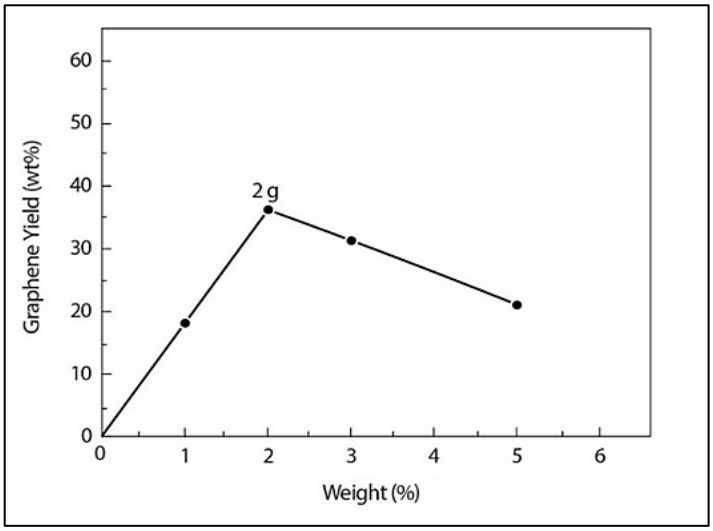

Figure 5: Effect of the initial amount of graphite on the yield of graphene

3.1.3 Surfactants

In this study, the experiments applied sodium hexametaphosphate and sodium lignosulfonate as surfactants. These surfactants form a weak bond with graphite, decreasing the extra energy and, as a result, lowering the tendency of graphene sheets to another bonding. The addition of surfactant results in the better exfoliation of graphite and long-term stabilization of the resulting graphene [31]. According to the results of the experiments, fewer layers and a higher yield of graphene were provided by sodium hexametaphosphate. The reason for the better performance of sodium hexametaphosphate compared to sodium lignosulfonate is related to this material's structure and chemical properties. Sodium hexametaphosphate has 6 double bonds and, thus, has a greater inherent ability to avoid re-stacking graphene layers. To explain the exfoliation mechanism of sodium hexametaphosphate, it can be said that sodium hexametaphosphate is a mixture of metaphosphates with 6 double bonds. Heating sodium hexametaphosphate produces monosodium orthophosphate and monosodium pyrophosphate compounds used in industry as precipitation inhibitors and dispersant agents. Still, sodium lignosulfonate is a natural polymer derived from lignin. In a chemical process called sulfonation, lignin is converted to sodium lignin sulfonate, and by attaching a sulfate functional group to it, the solubility of lignin increases during the sulfonation process. The problem with sodium lignosulfonate is that at the end of the process, due to the very high pressure of the separation process, insoluble cellulose materials and salts that remain from sodium lignosulfonate are separated from the graphite layers and cause the graphene layers to be placed on top of each other again. Thus, sodium hexametaphosphate has a greater intrinsic ability to prevent the re-stacking of graphene layers than sodium lignosulfonate [32].

Raman spectroscopy was performed to further investigate the effect of the mentioned surfactants on the quality of the resulting graphene. The quality of graphene can be evaluated by calculating the intensity ratio of 2D-band to G-band (I_{2D}/I_G) in Raman spectra. Also, the intensity ratio of D-band to G-band (I_D/I_G) can be used to measure the number of structural defects in graphene. The D-band is associated with structural defects or hexagonal symmetry breaking of disordered graphite. The D-band becomes stronger for graphene as the graphene becomes thinner and smaller in size. The G-band is related to phonon vibrations in SP^2 carbon materials. The shape and position of different peaks in the Raman spectrum can be used to determine the number of graphene layers. For fewer layers, the 2D-band shifts to a lower wavenumber becomes more symmetrical and increases in intensity. The weak D-band in the Raman spectrum of graphene is due to the structural defects of raw graphite, and the slight increase in the intensity of the D-band of graphene compared to graphite is attributed to the reduction in the size of the graphene sheets. After the process, the corners of the graphene sheets also appear as defects in the D-band of the Raman spectrum. So, as the graphene sheets become smaller, the contribution of the corners to the Raman spectrum increases compared to the carbon atoms of the main sheet, increasing the I_D/I_G ratio [33-35].

Table 5 shows the results of Raman spectroscopy for raw graphite and multilayer, bilayer, and monolayer graphene based on the literature [36].

Table 5: Characteristics of graphite and graphene evaluated by Raman spectroscopy [36]

	Peak wavenumber (cm^{-1})			I_D/I_G	I_{2D}/I_G
Material	**D-band**	**G-band**	**2D-band**		
Graphite	1343	1587	2720	0.17	0.42
Multilayer graphene	1348	1585	2718	0.23	0.58
Bilayer graphene	1352	1584	2717	0.31	0.61
Monolayer graphene	1356	1583	2716	0.35	0.63

Figure 6A shows the Raman spectrum of graphite and graphene precursors. Figure 6B shows the Raman spectrum of the original graphite. Figure 6C and D are graphite synthesized using sodium hexametaphosphate and sodium lignosulfonate.

According to Figure 6C and D, sodium hexametaphosphate provides a larger I_{2D}/I_G than sodium lignosulfonate, indicating the synthesis of graphene with fewer layers and higher quality. According to Figure 6C and D, it can be seen that the growth of I_{2D}/I_G and the very low peak range of the D-band, as well as the number of the 2D-band, show that the graphene has been synthesized with a higher quality. A small shoulder of the G-band at 1620 cm^{-1} corresponding to the D-band is observed, which is consistent with the observation of a strong D-band in the graphene sample. Also, the shape and position of the two-dimensional band are often used to identify the layer number (mainly for those with less than 3 layers) [35,36]. The value of relative intensity (I_{2D}/I_G) of multilayer graphene is 0.58, which indicates that graphene is less than 3 layers, which is consistent with AFM results. Furthermore, a slight blue shift in the 2D-band (from 2720 to 2716 cm^{-1}) is observed, proving that the graphite has been successfully exfoliated in $scCO_2$.

The highest I_D/I_G in graphene samples obtained by the $scCO_2$ method are 0.31 and 0.35, much lower than the corresponding values reported using other graphene synthesis methods. For example, in synthesizing graphene using a chemical method that includes oxidation and reduction processes, the I_D/I_G ratio is higher than 1, meaning that the graphene structural defects resulting from the chemical method are more than those obtained by the $scCO_2$ [37].

Figure 7 shows the effect of adding sodium hexametaphosphate and sodium lignosulfonate surfactants to graphite. So, according to Table 5, it was found that the lower the number of G-bands, the thinner graphene, is formed. According to Table 5 and Figure 7, it was understood that due to the addition of sodium hexametaphosphate, the G-band moved from 1587 cm^{-1} (graphite) to 1583 cm^{-1} (monolayer graphene), but due to the addition of sodium lignosulfonate to 1584 cm^{-1} (bilayer graphene) is reached, which shows the better performance of sodium hexametaphosphate in the formation of monolayer graphene. According to the mentioned material about the inherent and superior properties of sodium hexametaphosphate in converting graphite to graphene compared to sodium lignosulfonate, the effect of adding these two surfactants on graphene efficiency was investigated in Figure 8. By adding sodium hexameta- phosphate and sodium lignosulfonate, the graphene yield was 53% and 47%, respectively, which indicates the better performance of sodium hexametaphosphate.

3.1.4 Co-solvents

In general, the addition of co-solvent increases the polarity. The $scCO_2$ is nonpolar, so adding co-solvent increases the polarity and solubility of this fluid, which improves the interaction between graphite and the $scCO_2$ and improves the penetration of the supercritical fluid. The penetration into the graphite layers increases, and more graphene is obtained [38,39]. Different co-solvents such as NMP, DMF, and Isopropanol were applied in this study because they cover a wide range of polarities. Among the utilized co-solvents, NMP and DMF performed better than Isopropanol since they have higher dielectric constants. By preventing the re-accumulation of graphene layers and maintaining their stability, NMP and DMF result in a lower d-spacing between graphitic layers. Isopropanol has a low dielectric constant and cannot maintain the stability of the sheets, and as a result, the smaller sheets re-accumulate, and the number of graphene layers increases [40,41].

TEM images are used to study the changes in the structure of graphite after applying the supercritical process of carbon dioxide and the morphology of graphene layers. TEM uses electrons with very high voltage, and then the received signal is processed to display on a screen. Considering that the transmission electron microscope's operation is based on the electron beam's passage through the material, the darker areas indicate that fewer electrons have passed through this part of the material. In other words, the dark areas in the TEM images indicate the higher density of the material, which prevents the passage of the electron beam. Thus, the darkness of the graphite particles in the images is due to the difficulty of penetrating the electron beam into their thick structure, indicating the accumulation of many graphene layers in the graphite mass. In other words, monolayer graphene can be considered as a transparent film based on TEM properties. With the help of TEM images, a detailed analysis of the morphology of graphene layers is possible. The lateral size of the graphene layers in these images ranges from several hundred nanometers to several micrometers. Compared with the TEM images of graphite, the exfoliated graphene layers are very transparent, which shows that the thickness was greatly reduced, and the supercritical fluid effectively carried out the graphite exfoliation process. With the help of TEM images and careful observation of the corners of the graphene layers, the number of layers can be determined. Thus, the different layers in the corners can be seen as parallel lines [42].

TEM images of samples obtained from three different types of components are shown in Figure 9. It was found that monolayer and multilayer graphene can be obtained by exfoliation of graphite in DMF (Figure 9A), NMP (Figure 9B) and Isopropanol (Figure 9C) with the help of $scCO_2$. A folded monolayer graphene can be observed, as shown in Figure 9A. An electron diffraction pattern of the typical selected area (inset in Figure 9A and B) demonstrates that the graphene sheet is well crystallized in a hexagonal symmetry structure, which confirms that there are no distortions in the products during the exfoliating process. A Surface wrinkle bilayer and a folded graphene are shown in Figure 9B.

In other words, Figure 9A shows the view of graphene obtained with DMF co-solvent, from which it can be seen that the graphene sheet is thin and transparent, there is no apparent aggregation phenomenon with DMF co-solvent, and the lateral size of the resulting graphene was large and monolayered. Figure 9B shows the view of graphene obtained with NMP co-solvent, from which it can be seen that the obtained graphene sheet is thin, large, and transparent, but in some places, the sheets are folded and wrinkled, which shows It has two layers of graphene. It can be seen from Figure 9C that the use of isopropanol co-solvent leads to the thickening of the graphene sheet and the phenomenon of irregular stacking can be clearly seen, which means the fragments have a relatively large aspect ratio and the lateral size was about a few microns.

Also, in Figure 10, the effect of adding different solvents on graphene yield can be seen. As it is known, the graphene yield is 42% in the presence of DMF, 25% in the presence of NMP, and 10% in the presence of Isopropanol.

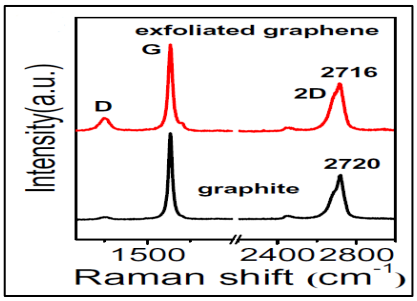

(A)

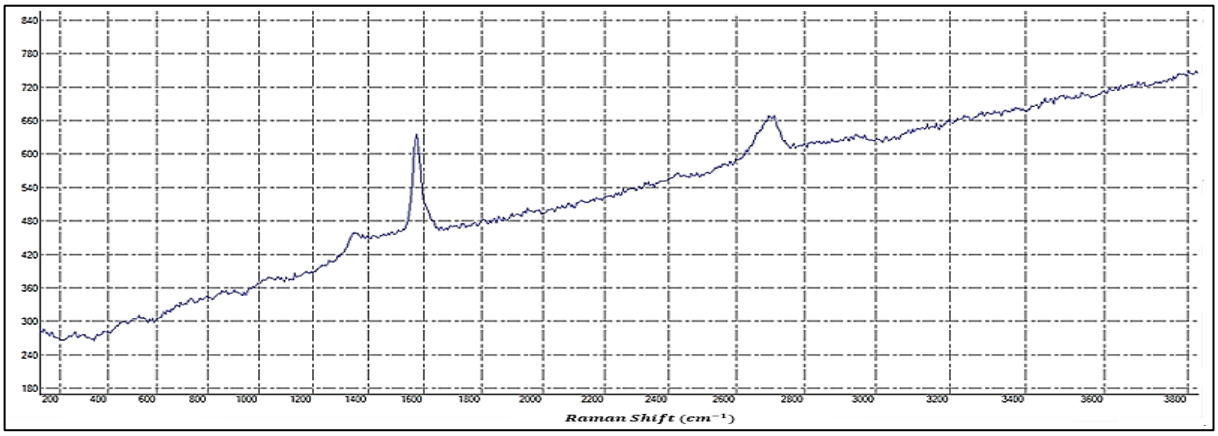

(B)

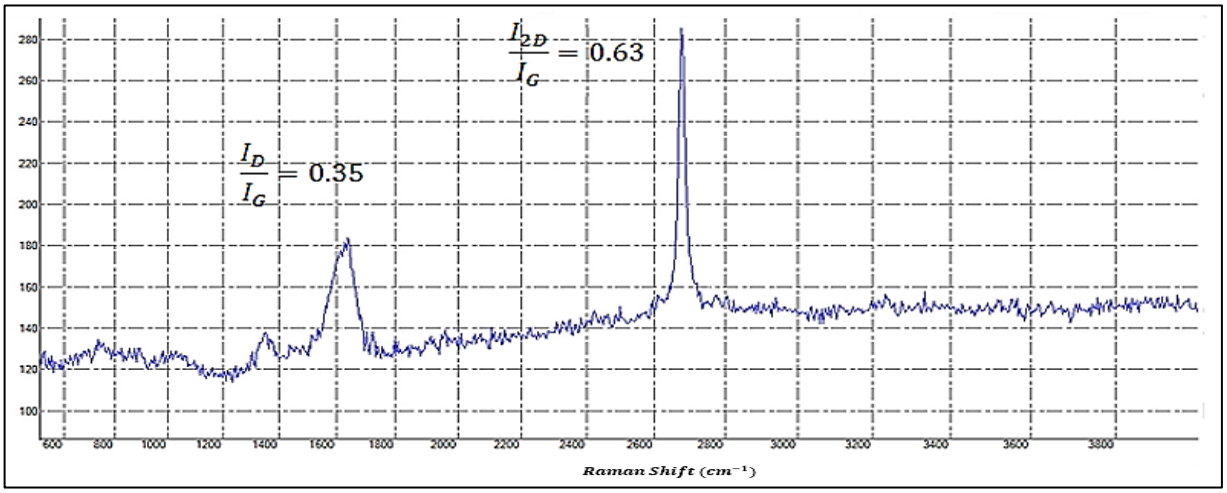

(C)

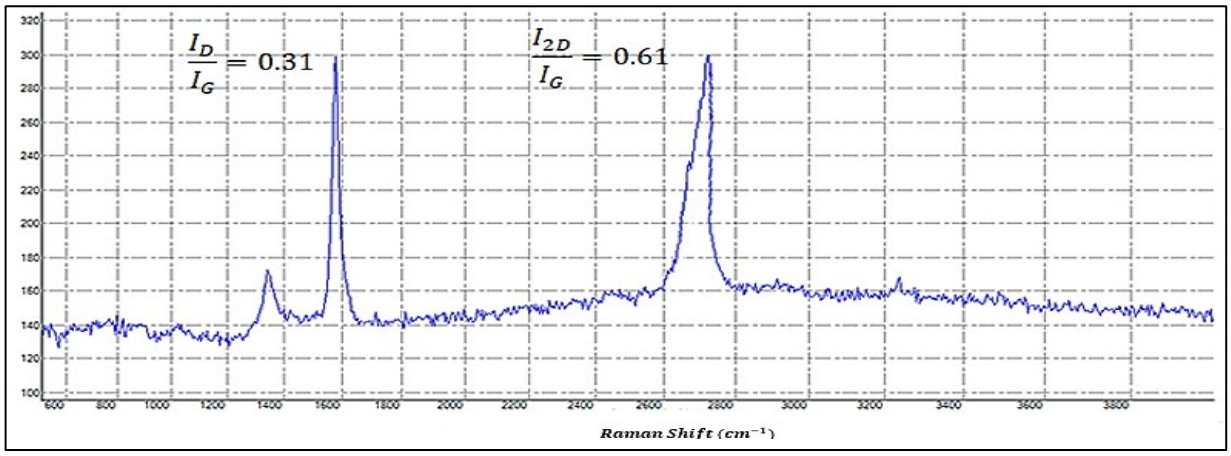

(D)

Figure 6: Raman spectrums for (A) Raman spectra of graphite and graphene. Reproduced with permission (B) raw graphite, (C) monolayer graphene obtained using sodium hexametaphosphate, and (D) bilayer graphene obtained using sodium lignosulfonate [37]

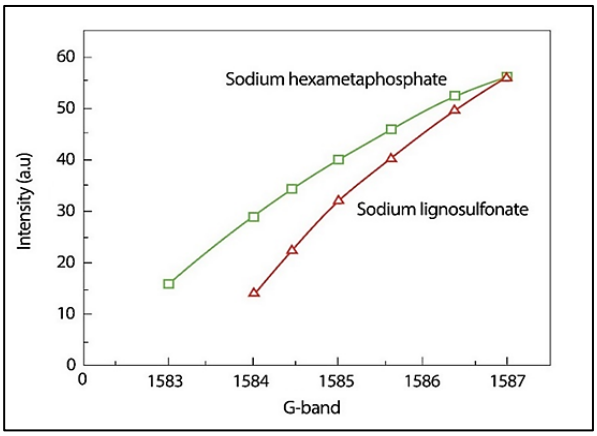

Figure 7: Effect of adding surfactants on G-band's intensity

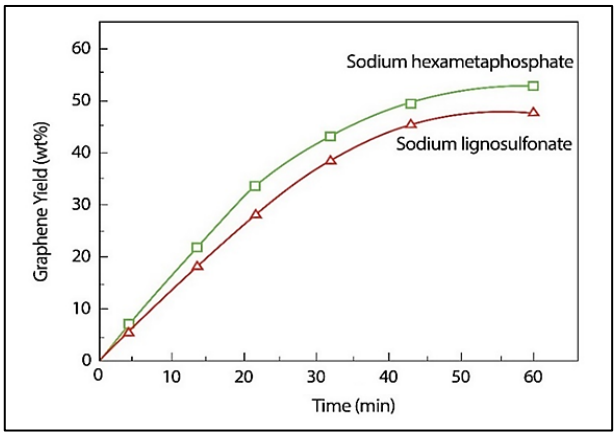

Figure 8: Effect of adding surfactants on the yield of graphene

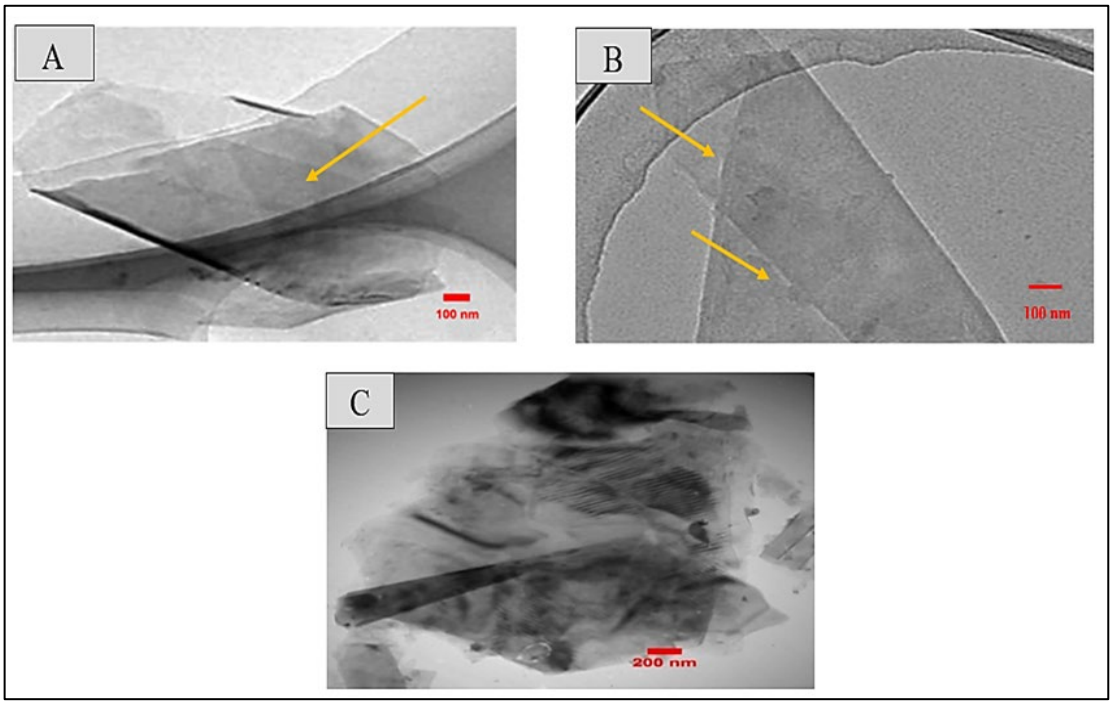

Figure 9: Effect of adding different co-solvents on the number of graphene layers: (A) DMF (monolayer graphene), (B) NMP (bilayer graphene), and (C) Isopropanol (multilayer graphene)

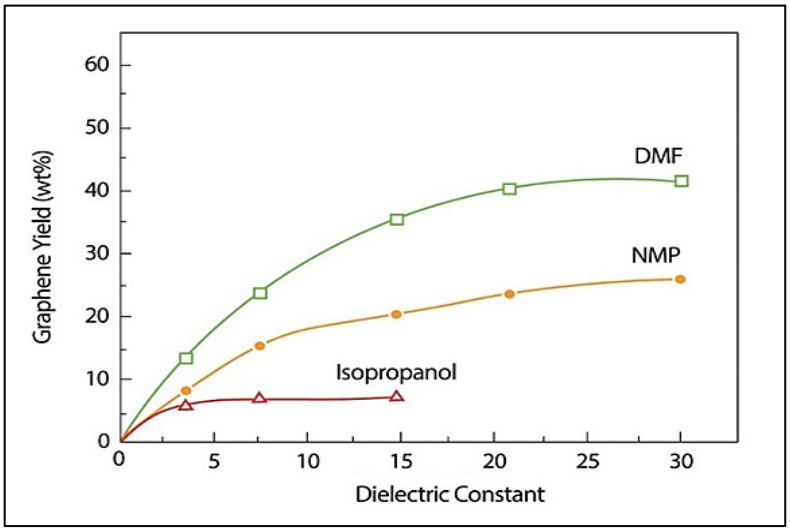

Figure 10: Effect of adding different co-solvents on the yield of graphene

3.1.5 Exfoliation duration in the cell

To investigate the effect of exfoliation time inside the device on graphene yield, the operating conditions were set to the optimal temperature and pressure (50°C and 250 bar). By reducing the sample placement time inside the cell, $scCO_2$ and graphite absorbed more shear energy and reduced the interaction between adjacent layers of graphite, resulting in higher efficiency. Further, the increase in yield by prolonging the cutting time for more than 1 hr was small, indicating that 1 hr is enough to achieve complete exfoliation. In fact, prolonging the exfoliation for more than 1 hr leads to the accumulation and cracking of the graphene layers and increases the thickness of the sheets. In this case, the exfoliated layers can re-accumulate and reduce the graphene yield [43].

Figure 11 shows the effect of processing time on the thickness of graphene sheets. As mentioned earlier, in the TEM test, the graphene layers can be counted due to the very high resolution, which shows that the thickness has been greatly reduced and the graphite exfoliation process by the supercritical fluid has been very effective. In Figure 11A, with 1 hr of placing the sample inside the graphene device, 1-3 layers were observed, and in Figure 11B, with 2 hr of placing the sample inside the graphene device, 10-15 layers were observed. Black areas say very high accumulation of graphene layers on top of each other and re-formation of graphite. The results showed that graphene with fewer layers and higher quality was obtained within 1 hr, as shown in Figure 12. When the exfoliation time in the cell was reduced from 2 hr to 1.5 and 1 hr, the graphene yield increased from 10% to 17% and then 20%.

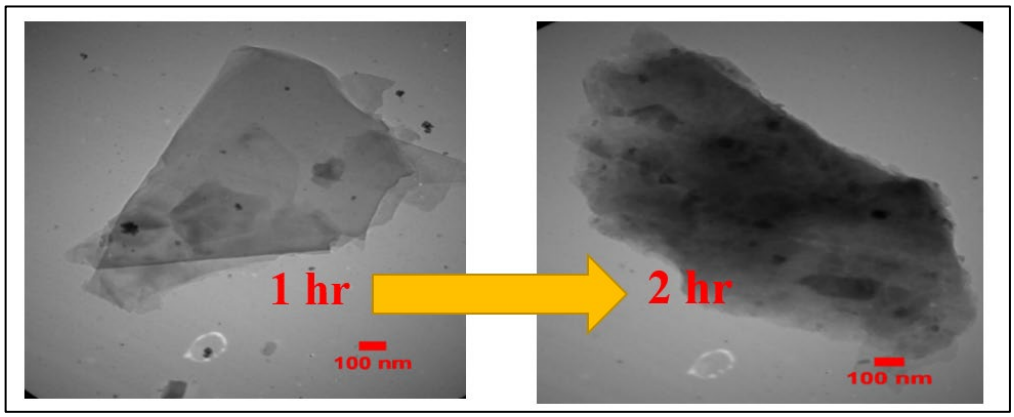

Figure 11: TEM images of graphene samples obtained: (A) after 1 hr, and (B) after 2 hr

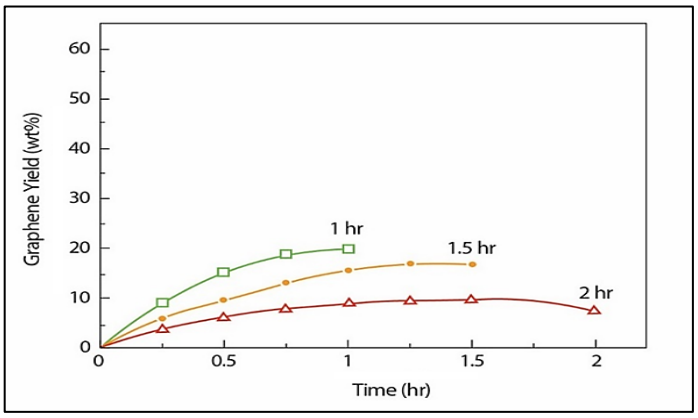

Figure 12: Effect of exfoliation time on the yield of graphene

3.1.6 Carbon dioxide discharge rate

Another important parameter of graphene formation is the discharge rate of carbon dioxide from the supercritical fluid device. In longer degassing (30 sec), the $scCO_2$ has enough time to destroy the van der Waals force between the graphite layers and form graphene sheets. But in fast discharge (5 and 17.5 sec), due to the short gas discharge time as well as the high pressure and speed of the supercritical fluid, the carbon dioxide moved irregularly in all directions as a result of all the power of the carbon dioxide to remove the force, van der Waals is not used. So, the production efficiency of graphene decreases. The longer the carbon dioxide gas is discharged (30 sec), the higher quality thin layer graphene is produced. However, an outgassing time of more than 1 minute is also not recommended because the exfoliated graphene sheets can re-aggregate to form graphite [44].

Figure 13 shows the effect of carbon dioxide discharge rate on the thickness of graphene sheets. In Figure 13A, the TEM image shows the discharge time of carbon dioxide gas from the device for 5 sec, and the black dots represent 10-15 layers of graphene. The Figure 13B is taken at a discharge time of 30 sec, and the transparent dots represent mono/bilayer graphene. Figure 14 shows the effect of the carbon dioxide gas discharge time parameter from the device on the efficiency of graphene. As can be

seen, in the discharge time of 5 sec, the efficiency of graphene is 5%. In the discharge time of 17.5 sec, the efficiency of graphene is 7.5%, and in the discharge time of 30 sec, the efficiency of graphene is 10%.

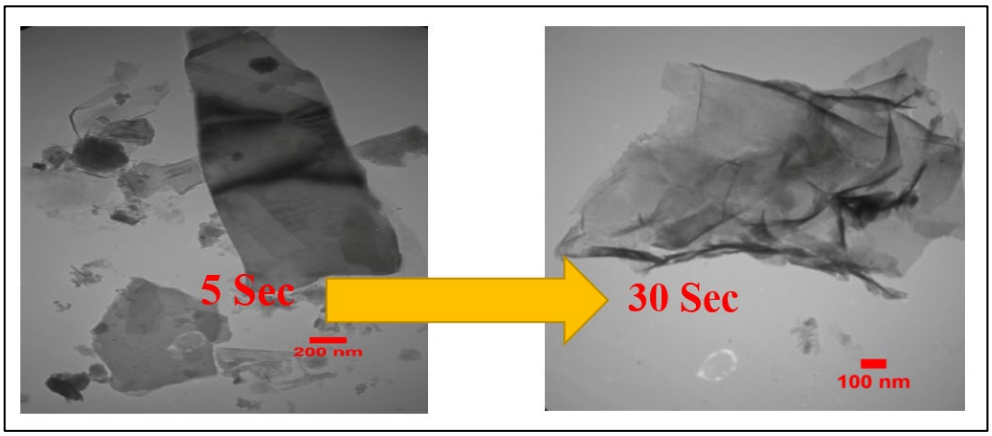

Figure 13: TEM images of graphene samples obtained: (A) after the gas was discharged in 5 sec, and (B) after the gas was discharged in 30 sec

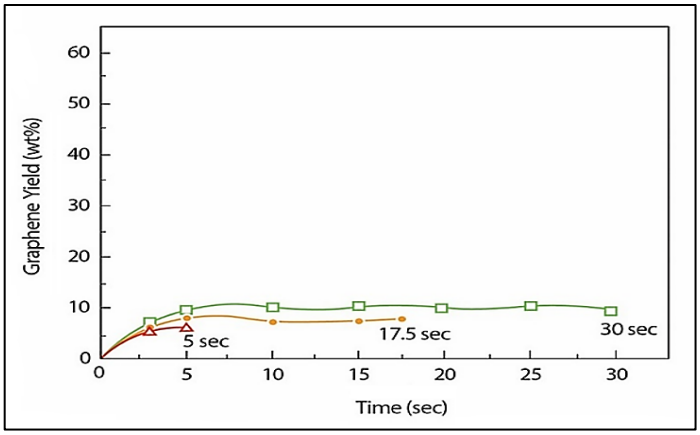

Figure 14: Effect of gas discharge duration on the yield of graphene

3.1.7 Ultrasonication time and power

About the effect of optimal ultrasound power, carbon dioxide, and graphite molecules absorb more energy the higher the power. This intensifies the movement of the carbon dioxide molecules between the graphite layers and causes the van der Waals force to weaken and break down. Creating more space between the resulting graphite layers and mono/multilayer graphene exfoliation is performed [45]. About the effect of optimal ultrasonic time, it can said that at time zero, when the ultrasonic operation has not yet started, the graph efficiency is zero. As ultrasonic time increases, carbon dioxide molecules have more opportunities to disperse between graphite layers, resulting in more graphite detachment. The reason for the slow growth of the exfoliation power after the optimum time can be attributed to the limitation of the amount of carbon dioxide in the reactor. Increasing the optimal ultrasound power and time leads to structural defects in the graphene. Therefore, the device must operate at optimum time and optimum power. In fact, with optimal time and power, the number of layers and the lateral sizes of the graphene layers can be controlled so that the number of layers and the size of the obtained graphene reach their lowest value [46]. In this study, the optimal time and power of ultrasonic operation were determined to be 120 min and 240 W, respectively.

Figure 15A and B shows the effect of not using/using ultrasonic, respectively. As can be seen, if the ultrasonic operation is not performed, the graphene layers will sit on top of each other and form graphite.

In Figure 16A, the effect of ultrasonic operation up to 300 W power was investigated. As can be seen, by increasing the ultrasonic power from 60 W to 240 W, the efficiency of graphene increases from 25% to 40%, and by increasing the power to 300 W, the efficiency decreases from 40% to 28%. In Figure 16B, the effect of ultrasonic time up to 240 min was investigated. As can be seen, by increasing the ultrasonic time from 60 min to 120 min, the graphene efficiency increases from 10% to 20%. Still, by increasing the time to 180 min, the efficiency decreases to 17%, and to 240 min, the efficiency decreases to 12%.

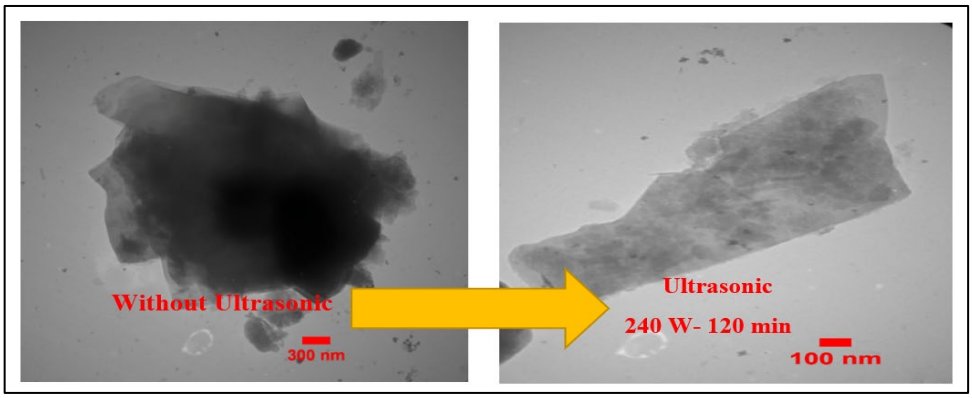

(A) **(B)**

Figure 15: TEM images of graphene samples obtained: (A) in the absence of ultrasonication, and (B) by ultrasonication at 240 W for 120 min

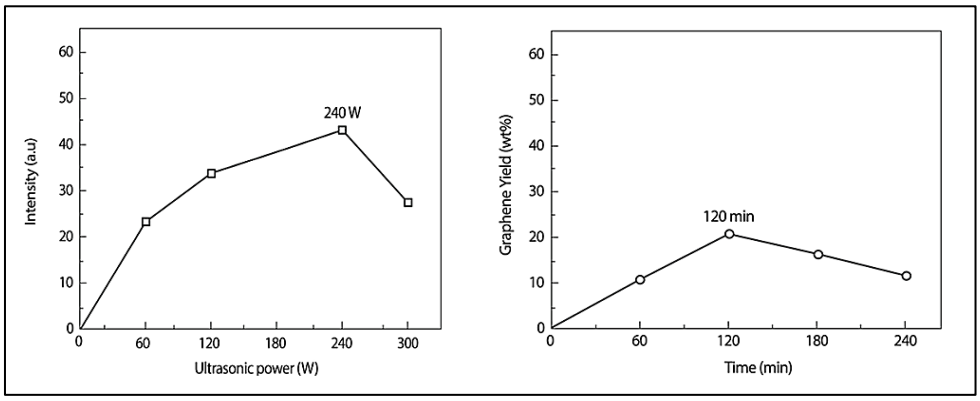

(A) **(B)**

Figure 16: Effect of ultrasonication time (A) and ultrasonic power (B) on the yield of graphene

3.1.8 Centrifugation time and power

Due to moderate ultrasound and centrifugation, the semi-agglomerated graphene can be dispersed on one side, and the unstriped graphite can be separated on the other. Also, to the large graphene grains, the dispersed phase usually contained small flakes and graphite crystals that had to be removed by centrifugation. We know that a lower centrifugal velocity leads to a higher graphene concentration because thicker graphene sheets remain in the supernatant. At the same time of centrifugation, the number of graphene layers obtained only by increasing the speed of centrifugation definitely became less and less [47].

Figure 17A and B shows the effect of not using/using centrifuge operation on graphene formation, respectively. According to Figure 17A and B and the above explanation about the centrifuge operation, it was found that if the centrifuge operation is not done at the optimal speed and time, the graphene efficiency will decrease. Figure 18A and B shows the effect of centrifuge time and speed on graphene efficiency. According to this Figure, it is clear that the use of centrifuge with 1000 rpm for 1 h resulted in the highest graphene efficiency (25%) and graphene A thicker layer was separated, resulting in a well-understood decrease in graphene concentration.

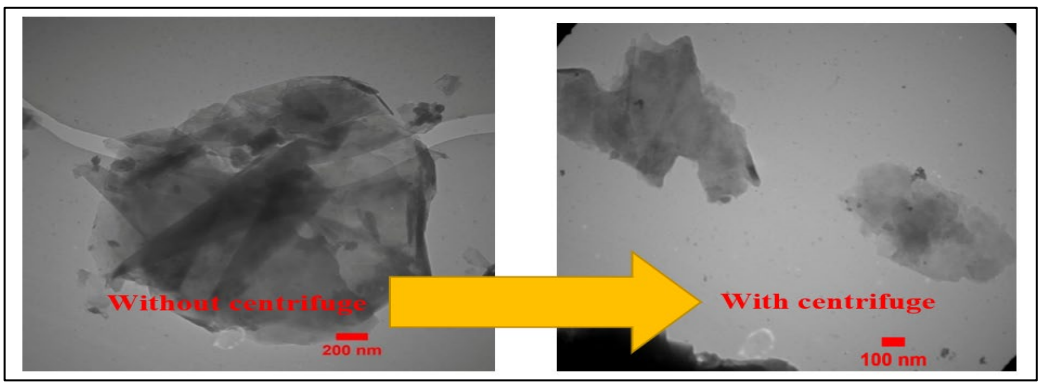

(A) **(B)**

Figure 17: TEM images of graphene samples obtained: (A) in the absence of centrifugation, and (B) by centrifugation at 1000 rpm for 60 min

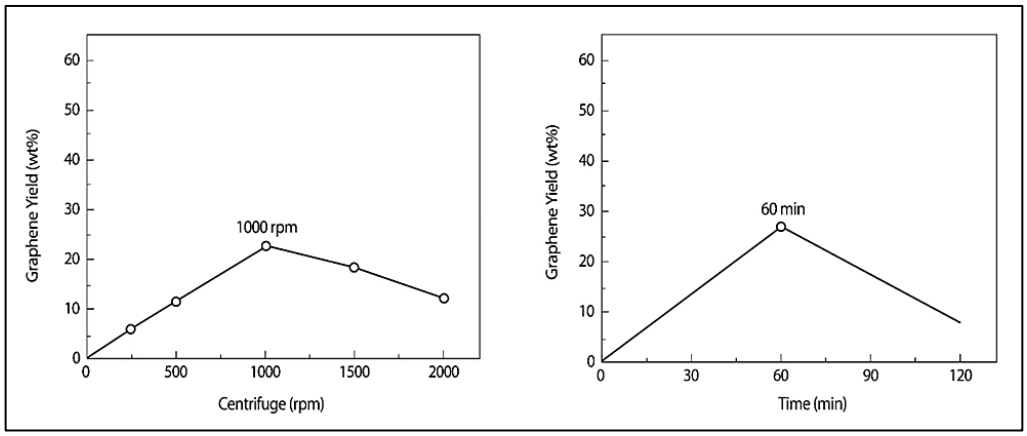

(A) **(B)**

Figure 18: Effect of centrifugation speed (A) and time (B) on the yield of graphene

3.2 Properties of Graphene Obtained at Optimal Operating Conditions

Different parameters affecting the yield of graphene obtained through graphite exfoliation using $scCO_2$ were discussed in Section 3.1. According to the obtained results, the optimal operating conditions for achieving the maximum graphene yield in the laboratory are summarized in Table 6.

Table 6: Optimal conditions for obtaining a maximum yield of graphene

Parameter	Optimal condition
Temperature	50˚C
Pressure	250 Bar
Initial graphite amount	2 g
Surfactant	Sodium hexametaphosphate
Co-solvent	DMF
Exfoliation duration in the cell	1 hr
CO_2 discharge duration	30 Sec
Ultrasonication time and power	120 min at 240 W
Centrifugation time and speed	60 min at 1000 rpm

The graphene obtained using the operating conditions mentioned in Table 6 was characterized through XRD spectroscopy and AFM. XRD spectrums of raw graphite and graphene samples synthesized using sodium hexametaphosphate and sodium lignosulfonate are depicted in Figure 19. The position of the main peak of these spectrums is tabulated in Table 7. The position of the main peaks of graphite and monolayer and bilayer graphene reported in the literature are also given in Table 7 for comparison.

To further explain the meaning of the XRD test, it can be said that when X-rays are emitted from the XRD device onto a material, they can act like a ((fingerprint)) to identify a material. To this end, XRD analyses of graphite and graphene samples and a comparison between them were performed to further investigate the structural changes of graphite after using a $scCO_2$. Figure 19A shows the prototype of graphite and graphene. According to Figure 19A and the XRD test of purchased graphite in Figure 19B and comparing these two Figures, it was found that the primary graphite had very high purity. The primary graphite has a very high purity. By comparing Figure 19C and D with Figure 19A, it was also found that the position of the XRD peak in the spectrum of graphene is similar to that of graphite. Still, the intensity of the peak in the XRD pattern is similar to that of graphene and is greatly reduced compared to graphite. This significant decrease is related to the decrease in the density of graphite layers. In other words, due to the very thin layers formed after the exfoliation process, the intensity of the (002) peak in the graphite decreased significantly, showing that the extraction of graphene using sodium hexametaphosphate was successfully performed lignosulfonate and it was converted into mono/bilayer graphene, respectively [48].

Table 7: Position of the main XRD peaks of graphite and graphene in the present study and the previous literature [48]

Material	2θ (˚) in the current study	2θ (˚) in the previous literature
Graphite	26.66	26.66
Monolayer graphene	26.48	26.48
Bilayer graphene	26.44	26.45

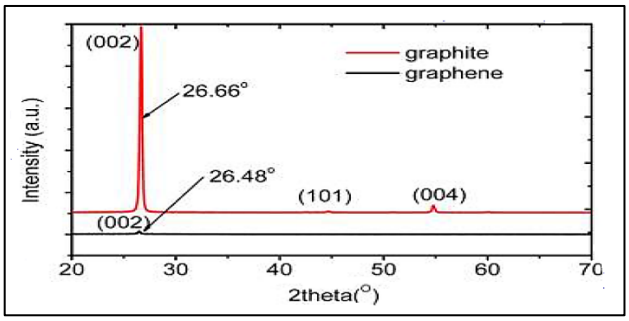

(A)

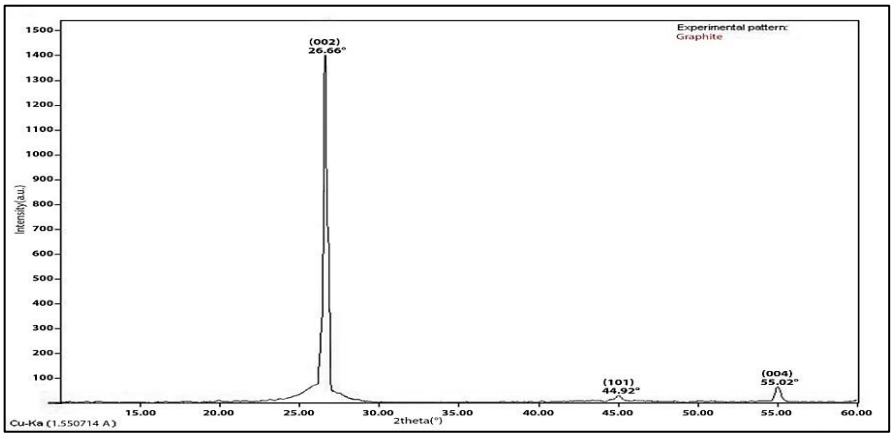

(B)

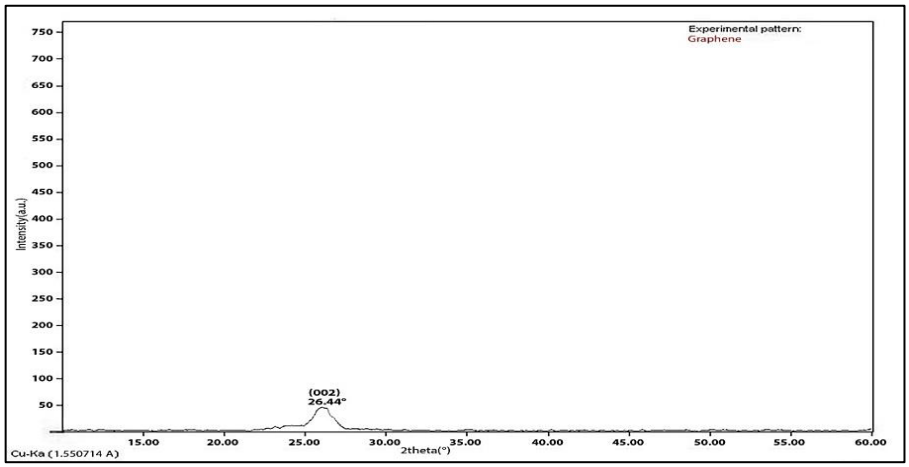

(C)

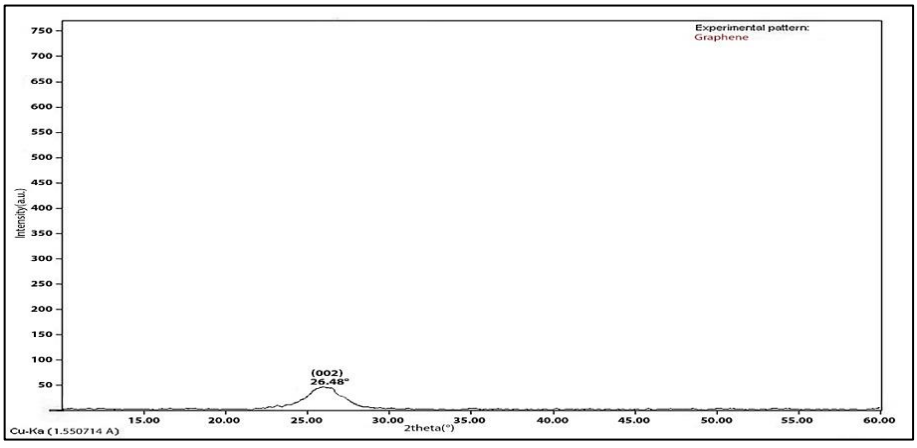

(D)

Figure 19: (A) XRD patterns of initial graphite and graphene, XRD spectrums of (B) raw graphite, (C) monolayer graphene synthesized using sodium hexametaphosphate, and (D) bilayer graphene synthesized using sodium lignosulfonate [48]

A promising method for determining the number of graphene layers is the investigation of AFM height profiles obtained for graphene samples. Figure 20A and B shows the AFM images and height profiles of graphene samples placed on a mica substrate. As can be seen, the graphene samples synthesized using sodium hexametaphosphate (Figure 20A) and sodium lignosulfonate (Figure 20B) have an average thickness of 1.5 and 2.5 nm, which correspond to monolayer and bilayer graphene [49].

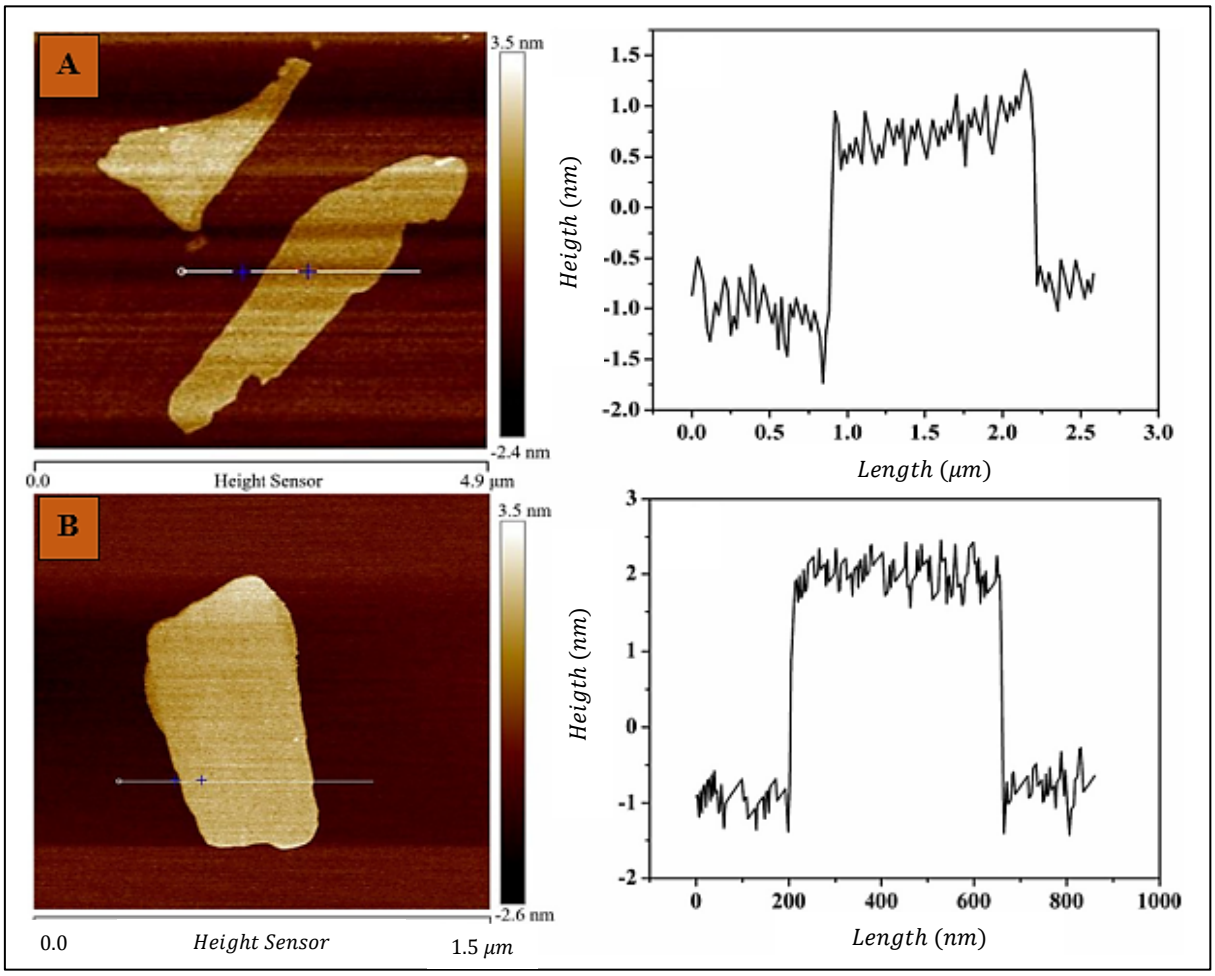

Figure 20: AFM images of surface topography and height profiles of graphene obtained at optimal conditions: (A) monolayer graphene synthesized using sodium hexametaphosphate and (B) bilayer graphene synthesized using sodium lignosulfonate

With the help of Design Expert software and conducting tests in the laboratory, the effect of operating parameters such as temperature, pressure, the initial amount of graphite, adding a surfactant and co-solvents, the duration of exfoliation in the cell, the duration of gas discharge, the duration of time and power of the ultrasound and the duration of time and speed of the centrifuge were evaluated on the efficiency and properties of the product and the optimal conditions were determined.

Finally, for a better comparison, the optimal values predicted by the Design Expert software and the results of the experiments performed in the laboratory are given in Table 8.

Table 8: Optimal values predicted by Design Expert software and experiments taken in the laboratory

Parameters	Factor	Optimal values predicted by Design Expert software	Optimal values obtained from experiments in the laboratory
Temperature	A	45 ℃	50 ℃
Pressure	B	155 Bar	250 Bar
Exfoliation duration in the cell of the supercritical device	C	1.5 hr	2 hr
Carbon dioxide discharge time	D	17.5 Sec	30 Sec
Amount of DMF	E	0.1 g	0.1 g
Amount of sodium hexametaphosphate	F	0.1 g	0.1 g
Initial amount of graphite	G	3 g	2 g

4. Conclusion

In this article, a new method for the preparation of mono/bilayer graphene using $scCO_2$ was presented. To improve the quality of the graphene produced, temperature, pressure, graphite quantity, solvent, and surfactant parameters were checked and adjusted during the exfoliation process. In addition, the time to introduce the graphite sample into the supercritical cell, release carbon dioxide gas from the instrument, and perform ultrasonic and centrifuge operations were optimized. Characterization of the synthesized graphene was performed by TEM, AFM, XRD, and RAMAN spectroscopy. The results confirmed that the $scCO_2$ could penetrate between the graphite layers at high speed and high pressure and separate the graphite layers well. The authors believe that the use of $scCO_2$ fluid in the synthesis of graphene has numerous advantages, such as high permeability, low viscosity, short extraction time, easy product recovery, environmental friendliness, and the elimination of the use of toxic and expensive chemicals will be used in the near future to make the method superior to other common methods of graphene production. With the help of supercritical fluid extraction, new products with special properties and high purity can also be manufactured and marketed commercially.

Acknowledgments

We gratefully acknowledge support from the High-Performance Computing Centre of Ferdowsi University of Mashhad.

Author contributions

Conceptualization, S. Saeedi and J. Sargolzaei; Software, S. Saeedi; writing—original draft preparation, J. Sargolzaei and S. Saeedi; writing—review and editing, J. Sargolzaei; supervision, J. Sargolzaei; All authors have read and agreed to the published version of the manuscript.

Funding

This research received no specific grant from any funding agency in the public, commercial, or not-for-profit sectors.

Data availability statement

The data that support the findings of this study are available on request from the corresponding author.

Conflicts of interest

The authors declare that there is no conflict of interest.

References

[1] M. Yi, Z. Shen, A review on mechanical exfoliation for scalable production of graphene, J. Mater. Chem. A, 35 (2015) 11700-11715. https://doi.org/10.1039/C5TA00252D

[2] S.K. Tiwari, S. Sahoo, N. Wang, A .Huczko, Graphene research and their outputs: Status and prospect, J. Sci. Adv. Mater. Devices., 5 (2020) 10-29. https://doi.org/10.1016/j.jsamd.2020.01.006

[3] G.M. da Costa, C.M. Hussain, Ethical, legal, social and economic issues of graphene, Compr. Anal. Chem., 91 (2020) 263-279. https://doi.org/10.1016/bs.coac.2020.08.010

[4] Q.B. Wang, J.Z. Yin, Q.Q. Xu, J.T. Zhi, Insightful understanding of shear-assisted supercritical CO_2 exfoliation for fabricating graphene nanosheets through the combination of kinetics and process parameters, Ind. Eng. Chem. Res., 59 (2020) 10967–10975. https://doi.org/10.1021/acs.iecr.0c01744

[5] Y. Yan, F.Z. Nashath, S. Chen, S. Manickam, S.S. Lim, H. Zhao, E. Lester, T. Wu, C.H. Pang, Synthesis of graphene: Potential carbon precursors and approaches, J. Nanotechnol. Rev., 9 (2020) 1284-1314. https://doi.org/10.1515/ntrev-2020-0100

[6] P.S. Owuor, A. Khan, C.L. Leon, S. Ozden, R. Priestley, C. Arnold, N. Chopra, C.S. Tiwary, Roadblocks faced by graphene in replacing graphite in large-scale applications, Oxf. open mater. Sci., 40 (2021)1-19. https://doi.org/10.1093/oxfmat/itab004

[7] H.C. Lee, W.W. Liu, S.P. Chai, A.R. Mohamed, A. Aziz, C.S. Khe, N.M.S. Hidayah, U. Hashim, Review of the synthesis, transfer, characterization and growth mechanisms of single and multilayer graphene, J. RSC Adv., 7 (2017) 15644-15693. https://doi.org/10.1039/C7RA00392G

[8] M. Li, S.K. Cushing, X .Zhou, S. Guo, N. Wu , Fingerprinting photoluminescence of functional groups in graphene oxide, J. Mater. Chem., 22 (2012) 23374-23379. https://doi.org/10.1039/C2JM35417A

[9] C. Liu, G. Hu, H. Gao, Preparation of few-layer and single-layer graphene by exfoliation of expandable graphite in supercritical N,N-dimethylformamide, J. Supercrit. Fluids, 63 (2012) 99-104. https://doi.org/10.1016/j.supflu.2012.01.002

[10] S. P. Sasikala, P. Poulin, C. Aymonier, Prospects of Supercritical Fluids in Realizing Graphene-Based Functional Materials, J. Adv. Mater., 28 (2016) 2663-2691. https://doi.org/10.1002/adma.201504436

[11] Z. Sun, Q. Fan, M. Zhang, S. Liu, H Tao, J. Texter, Supercritical Fluid-Facilitated Exfoliation and Processing of 2D Materials, Adv. Sci., 6 (2019) 1901084. https://doi.org/10.1002/advs.201901084

[12] B. Ahangari, J. Sargolzaei, Extraction of lipids from spent coffee grounds using organic solvents and supercritical carbon dioxide, J. Food Process. Preserv., 37 (2013) 1014-1021. https://doi.org/10.1111/j.1745-4549.2012.00757.x

[13] B. Ahangari, J. Sargolzaei, Extraction of pomegranate seed oil using subcritical propane and supercritical carbon dioxide, Theor. Found. Chem. Eng., 46 (2012) 258–265. https://doi.org/10.1134/S0040579512030013

[14] B. Ahangari, J. Sargolzaei, Supercritical Fluid Extraction of Oils from Pomegranate Seeds, J. Am. Oil. Chem. Soc., 94 (2017) 1415-1415. https://doi.org/10.1007/s11746-011-1789-9

[15] N.W. Pu, C.A. Wang, Y. Sung, Y.M. Liu, M.D. Ger, Production of few-layer graphene by supercritical CO_2 exfoliation of graphite, Mater. Lett., 63 (2009) 1987-1989. https://doi.org/10.1016/j.matlet.2009.06.031

[16] H Gao, G Hu, Graphene production via supercritical fluids, RSC Adv., 12 (2016) 10132-10143. https://doi.org/10.1039/C5RA15568A

[17] Z. Sun, Q. Fan, M. Zhang, S. Liu, H. Tao, J. Texter, Supercritical fluid-facilitated exfoliation and processing of 2D materials, Adv. Sci., 6 (2019) 1-34. https://doi.org/10.1002/advs.201901084

[18] D. Rangappa, K .Sone, M .Wang, U.K. Gautam, D. Golberg, H. Itoh, M. Ichihara, I. Honma,Rapid and direct conversion of graphite crystals into high-yielding, good-quality graphene by supercritical fluid exfoliation, Journal of Chem. Europe. Chem. Eur. J., 16 (2010) 6488-6494. https://doi.org/10.1002/chem.201000199

[19] H. Zhu, J. Yin, Study on cloud point pressure of $EmimTf_2N$ in supercritical carbon dioxide microemulsions based on non-ionic surfactant and role of solubilized water, J. Mol. Liq., 310 (2020) 113299. https://doi.org/10.1016/j.molliq.2020.113299

[20] H. Zhu, Y. Li, D. Zhou, Q. Xu, J. Yin, Molecular dynamics study on microstructure of supercritical CO_2 microemulsions containing ionic liquids, Colloids Surf. A Physicochem. Eng. Asp., 603 (2020) 125272. https://doi.org/10.1016/j.colsurfa.2020.125272

[21] W. Yu, Y. Liu, J. Yin, Separation of 1,3-propanediol using supercritical CO_2 microemulsion with non-ionic surfactant Ls-54: experiment and simulation, Chem. Eng. J., 273 (2015) 197-204. https://doi.org/10.1016/j.cej.2015.03.082

[22] R. Navik, H. Tan, Z. Liu, Q. Xiang, Y. Zhao, Scalable production of high-quality exfoliated graphene using mechanical milling in conjugation with supercritical CO_2, FlatChem, 33 (2022) 100374. https://doi.org/10.1016/j.flatc.2022.100374

[23] M. Kumar, H..S Farwaha, N. Ranjan, Use of Response Surface Methodology to Optimize the crystalline size of rice husk derived graphene produced by microwave process, IOP Conf. Ser.: Earth Environ. Sci., 1110,2023,012069. https://doi.org/10.1088/1755-1315/1110/1/012069

[24] Y.L. Leong, H.N. Lim, I. Ibrahim, Graphene in rubber formulations: a comprehensive review and performance optimization insights, Mol. Syst. Des. Eng., 8 (2023) 1229-1251. https://doi.org/10.1039/D3ME00082F

[25] A.A. AbdulRazak, Z.M. Shakor, S. Rohani, Optimizing Biebrich Scarlet removal from water by magnetic zeolite 13X using response surface method, J. Environ. Chem. Eng., 6 (2012) 6175-6183. https://doi.org/10.1016/j.jece.2018.09.043

[26] T. Al-Dahri, A.A.J. AbdulRazak, I.H. Khalaf, S. Rohani, Response surface modeling of the removal of methyl orange dye from its aqueous solution using two types of zeolite synthesized from coal fly ash, Mater. Express, 8 (2018) 234-244. https://doi.org/10.1166/mex.2018.1433

[27] B. Wu, X. Yang, A molecular simulation of interactions between graphene nanosheets and supercritical CO_2, J. Colloid Interface Sci., 361 (2011) 1-8. https://doi.org/10.1016/j.jcis.2011.05.021

[28] H. Gao, G. Hu, Graphene production via supercritical fluids, RSC Adv., 6 (2016) 10132-10143. https://doi.org/10.1039/C5RA15568A

[29] L. Li, J Xu, G. Li, X. Jia, Y. Li, F. Yang, L. Zhang, Preparation of graphene nanosheets by shear-assisted supercritical CO_2 exfoliation, Chem. Eng. J., 284 (2016) 78-84. https://doi.org/10.1016/j.cej.2015.08.077

[30] A. Hadi, J. Karimi-Sabet, S.M.A. Moosavian, Optimization of graphene production by exfoliation of graphite in supercritical ethanol: A response surface methodology approach, J. Supercrit. Fluids, 107 (2016) 92-105. https://doi.org/10.1016/j.supflu.2015.08.022

[31] L. Xu, J.W. McGraw, F. Gao, M. Grundy, Z. Ye, Production of High-Concentration Graphene Dispersions in Low-Boiling-Point Organic Solvents by Liquid-Phase Noncovalent Exfoliation of Graphite with a Hyperbranched Polyethylene and Formation of Graphene/Ethylene Copolymer Composites, J. Phys. Chem. C, 117 (2013) 0730–10742. https://doi.org/10.1021/jp4008009

[32] H. Zhao, X. Pang, Z. Zhai, Preparation and Antiflame Performance of Expandable Graphite Modified with Sodium Hexametaphosphate, Hindawi Publishing Corporation, J. Polym., 2015 (2015) 5. http://dx.doi.org/10.1155/2015/821297

[33] S.J. Goldie, S. Bush, J.A. Cumming, A Statistical Approach to Raman Analysis of Graphene-Related Materials: Implications for Quality Control, ACS Appl. Nano Mater., 3 (2020) 11229–11239. https://doi.org/10.1021/acsanm.0c02361

[34] A. Adetayo, D. Runsewe, Synthesis and Fabrication of Graphene and Graphene Oxide: A Review, Open Journal of Composite Materials., 9 (2019) 207-229. https://doi.org/10.4236/ojcm.2019.92012

[35] Z. Li, L. Deng, I.A. Kinloch, R.J. Young, Raman spectroscopy of carbon materials and their composites: Graphene, nanotubes and fibres, Prog. Mater. Sci., 135 (2023) 101089. https://doi.org/10.1016/j.pmatsci.2023.101089

[36] V.O. Yukhymchuk, M.Y. Valakh, O.M. Hreshchuk, Y.O. Havrylyuk, I.B. Yanchuk, A.V. Yefanov, Properties of Graphene Flakes Obtained by Treating Graphite with Ultrasound, Ukr. J. Phys., 62 (2017) 432-440. https://doi.org/10.15407/ujpe62.05.0432

[37] D. Lopez-Diaz, J.A. Delgado-Notario, V. Clerico, E. Diez, M.D. Merchan, M.M. Velazquez,Towards Understanding the Raman Spectrum of Graphene Oxide: The Effect of the Chemical Composition, Coatings, 10 (2020) 524. https://doi.org/10.3390/coatings10060524

[38] M.S. Khan, A. Shakoor, G.T. Khan, S. Sultana, A. Zia, A Study of Stable Graphene Oxide Dispersions in Various Solvents, J. Chem. Soc. Pak., 37 (2015) 62-67.

[39] Q. Li, Z. Zhang, C. Zhong, Y. Liu, Q. Zhou, Solubility of solid solutes in supercritical carbon dioxide with and without co-solvents, Fluid Phase Equilib., 207 (2003) 183-192. https://doi.org/10.1016/S0378-3812(03)00022-0

[40] V.B. Mbayachi, E. Ndayiragije, T. Sammani, S. Taj, E.R. Mbuta, A.U. Khan, Graphene synthesis, Characterization and its applications: A review, Results Chem., 3 (2021) 100163. https://doi.org/10.1016/j.rechem.2021.100163

[41] M. Yi, Z. Shen, S. Ma, X. Zhang, A mixed-solvent strategy for facile and green preparation of graphene by liquid-phase exfoliation of graphite, J. Nanopart. Res., 14 (2012)1-9. https://doi.org/10.1007/s11051-012-1003-5

[42] S.A. Bhuyan, M.D. Nizam Uddin, M. Islam, F. A. Bipasha, S.S. Hossain, Synthesis of graphene, Int Nano Lett., 6 (2016) 65-83. https://doi.org/10.1007/s40089-015-0176-1

[43] N. Liu, Q. Tang, B. Huang, Y. Wang, Graphene Synthesis: Method, Exfoliation Mechanism and Large-Scale Production, Crystals, 12 (2022) 25. https://doi.org/10.3390/cryst12010025

[44] L. Li, J. Xu, G. Li, X. Jia, Y. Li, F. Yang, L. Zhang, Preparation of graphene nanosheets by shear-assisted supercritical CO_2 exfoliation, Chem. Eng. J., 284 (2016) 78-84. https://doi.org/10.1016/j.cej.2015.08.077

[45] L.I. Silva, D.A. Mirabella, J.P. Tomba, C.C. Riccardi, Optimizing graphene production in ultrasonic devices, Ultrasonics, 100 (2020) 105989. https://doi.org/10.1016/j.ultras.2019.105989

[46] Z. Liu, R. Navik, H. Tan, Q. Xiang, M. Goto, Graphene-based materials prepared by supercritical fluid technology and its application in energy storage, J. Supercrit. Fluids,188 (2022) 105672. https://doi.org/10.1016/j.supflu.2022.105672

[47] S. Xu, Q. Xu, N. Wang, Z. Chen, Q. Tian, H. Yang, Reverse-Micelle-Induced Exfoliation of Graphite into Graphene Nanosheets with Assistance of Supercritical CO_2, Chem. Mater., 27 (2015) 3262–3272. https://doi.org/10.1021/acs.chemmater.5b00092

[48] N. Kumar, R. Salehiyan, V. Chauke, O.J. Botlhoko, K. Setshedi, M. Scriba, M. Masukume, S.S. Ray, Top-down synthesis of graphene: A comprehensive review, FlatChem, 27 (2021) 100224. https://doi.org/10.1016/j.flatc.2021.100224

[49] L. Saikam, P .Arthi, B. Senthil, M. Shanmugam, A review of exfoliated graphite: synthesis and applications, J.Inorg. Chem. Commun., 152 (2023) 110685. https://doi.org/10.1016/j.inoche.2023.110685